An experimental and theoretical study of the HOMO of W(CO)$_6$: Vibrational effects on the electron momentum density distribution

K. Liu, C.G. Ning *, Z.H. Luo, L.L. Shi, J.K. Deng **

Department of Physics and Key Laboratory of Atomic and Molecular NanoSciences of MOE, Tsinghua University, Beijing 100084, People's Republic of China

ARTICLE INFO

ABSTRACT

The unexpected higher intensity at low momentum region for HOMO of W(CO)$_6$ was investigated using electron momentum spectroscopy at various impact energies, as well as non-relativistic, scalar relativistic and spin–orbit relativistic DFT-B3LYP calculations. There was no evident difference between the experimental momentum profiles at various impact energies. It was found that the low frequency vibration of W(CO)$_6$ can evidently change the momentum profile. The semi-quantitative vibrational averaged calculations agreed well with the experimental results. Therefore, it was suggested that the unexpected higher intensity at low momentum regions was possibly due to the vibration effects.

© 2010 Elsevier B.V. All rights reserved.

1. Introduction

Electron momentum spectroscopy (EMS) [1–3], also known as (e, 2e) spectroscopy, is a powerful tool to investigate electronic structures of atoms and molecules. It can measure the binding spectrum and the electron momentum distribution for each individual orbital at the same time. The observed momentum distributions can be directly compared with the theoretical calculation under the assumptions of the Born, binary encounter, and plane wave impulse approximations (PWIA). This feature has made EMS have abilities to measure the orbital electron densities and evaluate basis sets and computational methods for quantum chemistry.

The volatile transition metal carbonyls, tungsten hexacarbonyl (W(CO)$_6$), well-known as precursor in organometallic chemistry and as a model for the bond between CO and metal surfaces [4], is an ideal molecular target for the gas phase EMS study. The only previous EMS investigation of the highest occupied molecular orbital (HOMO) of W(CO)$_6$ was performed by Rolke et al. [5] at impact energy of 1200 eV. A discernable discrepancy at low momentum region was found between the experimental momentum profiles and the calculations using non-relativistic methods in that work. Rolke et al. ascribed the discrepancy to the distorted wave effects. However, their measurement at only one impact energy cannot provide a definitive conclusion. Recently, such unexpected higher intensities at low momentum regions were also observed for several particular molecular orbitals [6–10], which have been attributed to distorted wave effects. By now, the distorted wave

impulse approximation (DWIA) calculation is still a challenge for molecules due to the multi-center system [11–13]. To test this hypothesis for W(CO)$_6$, it is more practical to measure the momentum distributions at different impact energies. In addition, the influence of relativistic effects also need to be taken into account considering the high-Z element W (Z = 74) in W(CO)$_6$ molecule.

In this Letter, we reported the momentum distributions of the HOMO of W(CO)$_6$ at the impact energies of 1200 and 2400 eV with a higher resolution and a higher statistical accuracy. The experimental momentum profiles were compared with the theoretical momentum profiles derived from non-relativistic, scalar relativistic and spin–orbit relativistic calculations using our new method [14]. The results showed that the calculations using the relativistic methods can provide a better description of experimental results than the non-relativistic method for W(CO)$_6$. Since the distorted effects and relativistic effects could not well explain the unexpected intensity at the lower momentum region for the HOMO, we suggested that it was very likely due to the vibrational effects. Our semi-quantitative calculations showed that the low frequency vibrational mode with a large amplitude nuclear motion at room temperature can evidently change the orbital momentum distributions.

2. Experimental and theoretical background

The details of our high resolution EMS spectrometer have been previously reported elsewhere [15,16]. Therefore, only a brief description is given here. Our spectrometer takes the symmetric non-coplanar geometry. In this geometry, the target are ionized by a high energy electron beam, and the two outgoing electrons have almost equal kinetic energies and equal polar angles θ ($\theta_1 = \theta_2 = 45°$) respect to the incoming electron beam. A double toroidal energy analyzer and two large position sensitive detectors

---

* Corresponding author. Fax: +86 10 62781604.
** Corresponding author. Fax: +86 10 62781604.
 E-mail addresses: ningcg@tsinghua.edu.cn (C.G. Ning), djk-dmp@tsinghua.edu.cn (J.K. Deng).

increases the collecting efficiency for the coincidental (e, 2e) events. An electron gun equipped with an oxide cathode working at much lower temperature than the generic filament cathodes is used to generate the electron beam with a low energy spread and a small divergence angle. In the present work, an energy resolution of $\Delta E = 0.68$ eV (full width at half maximum (FWHM)) can be obtained at the impact energy 1200 eV. The momenta of electrons prior to being knocked out can be determined through the out-of-plane azimuthal angle ϕ between the two outgoing electrons using the equation:

$$p = \left[(2p_1 \cos \theta - p_0)^2 + 4p_1^2 \sin^2 \theta \sin^2 \left(\frac{\phi}{2} \right) \right]^{1/2}, \tag{1}$$

where p_0 is the momentum of the incident electron, p_1 and p_2 ($p_1 = p_2$) are the momenta for the two outgoing electrons.

The plane wave impulse approximation (PWIA) gives a good description for the collision under the conditions of the high impact energy, high-momentum transfer, and negligible kinetic-energy transfer to the residual ion. Under the PWIA and target Kohn–Sham approximation (TKSA) in the framework of the density functional theory, the EMS differential cross section for randomly oriented gas-phase molecules is given by [17]

$$\sigma_{EMS} \propto \int d\Omega |\psi_j^{KS}(p)|^2, \tag{2}$$

where $\psi_j^{KS}(p)$ is the momentum space Kohn–Sham orbital for the jth electron. $\int d\Omega$ indicates the spherical average due to the randomly oriented gas phase target. According to the Eq. (2), EMS is able to image the electron density of individual orbital selected according to their binding energies.

To investigate the relativistic effects, Amsterdam Density Functional (ADF) 2008 program [18] was used to perform the relativistic and non-relativistic (NR) DFT calculations. The relativistic calculations include scalar relativistic (SR) and spin–orbit relativistic (SO) methods. The latter is one kind of two-component relativistic methods which can provide spin–orbit splitting components. By means of ADF, all calculations in the present work are performed using the standard hybrid Becke three-parameter, Lee–Yang–Parr (B3LYP) functional [19]. The NR calculations use the triple-ζ polarized basis sets (TZP) with frozen core shell up to the 4d level, while the relativistic calculations including SR and SO calculations use the triple-ζ doubly polarized basis sets specifically designed for the zero-order regular approximation [20] formalism (ZORA/TZ2P) without the frozen core. The optimized geometry of $W(CO)_6$ calculated by Ehlers and Frenking [21] is used for all the calculations, where $R_{W-C} = 2.0597$ Å and $R_{C-O} = 1.1655$ Å.

Theoretical momentum profiles calculations need Fourier transform and spherical integral on the wavefunctions in position space. So we use our newly developed program named ADFCOVT [14] and NEMS [22] program to generate theoretical momentum profiles. The molecular orbital generated using the spin–orbit relativistic ADF calculation has the following form:

$$\Psi(r) = \Psi_\alpha(r)\alpha + \Psi_\beta(r)\beta, \tag{3}$$

where α and β are the spin variables and orthogonal with each other. $\Psi_\alpha(r)$ and $\Psi_\beta(r)$ are the space wave function components for the spins α and β, respectively. The momentum distributions $|\Psi(p)|^2$ for the two-component molecular orbitals are obtained by the equation:

$$|\Psi(p)|^2 = |\Psi_\alpha(p)|^2 + |\Psi_\beta(p)|^2, \tag{4}$$

where $|\Psi_\alpha(p)|^2$ and $|\Psi_\beta(p)|^2$ are the momentum distributions for the spin α and β components.

The $W(CO)_6$ sample was obtained commercially and of 99.0% stated purity. The sample is solid, and can sublime at room temperature. Since the volatility is not sufficient, we put the sample probe directly inside the spectrometer. A heater with a variable power, typically 0.4 W, is employed to control the density of gaseous molecules. The temperature at the collision region is little higher than the room temperature, roughly 310 K as estimated. The measurement proceeds without further purifications. No impurity of the sample is evident in the binding-energy spectra.

3. Results and discussion

The tungsten hexacarbonyl ($W(CO)_6$) molecule contains 158 electrons and has an O_h symmetry point group. According to the scalar relativistic B3LYP/TZ2P calculation, the ground state electronic configuration can be written as

$$(core)^{78} \underbrace{(7t_{1u})^6(1t_{2u})^6(1a_{2u})^2(8a_{1g})^2(8t_{1u})^6(5e_g)^4}_{\text{inner valence}}$$

$$\times \underbrace{(9a_{1g})^2(6e_g)^4(9t_{1u})^6(10a_{1g})^2(7e_g)^4(3t_{2g})^6(10t_{1u})^6(2t_{2u})^6(1t_{1g})^6(11t_{1u})^6(4t_{2g})^6}_{\text{outer valence}}$$

The valence shell contains 17 molecular orbitals and can be divided into two sets: six inner valence and 11 outer valence orbitals. In the spin–orbit relativistic ADF calculations, each degenerate molecular orbital splits into two spin–orbit components.

The binding energy spectrum of $W(CO)_6$ in the region of 5–25 eV at the electron impact energy of 1200 eV is presented in Figure 1. With reference to high-resolution PES work [23], eight peaks can be resolved from the spectrum. The HOMO orbital $4t_{2g}$ is assigned to the first peak at 8.6 eV, which separates from other peaks clearly.

The experimental momentum profiles are extracted by deconvolving the same peak from the obtained binding-energy spectra at different azimuthal angles or momentum [1,3]. Theoretical momentum profiles are convolved the experiment resolution at $E_0 = 2400$ eV using a Monte Carlo method [24]. In order to compare the experimental momentum distributions with the theoretical ones, we need one common normalization factor for all bands. The present study uses one of the common normalization processes in the area of EMS. The factor is determined by the best fitting between the experimental summation of the outer valence orbital momentum profiles and the corresponding summation of the theoretical outer valence momentum distributions of $W(CO)_6$.
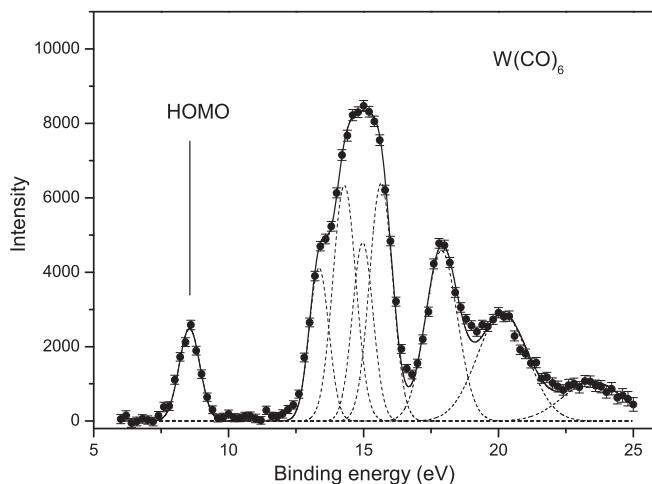

Fig. 1. Experimental binding energy spectrum summed over all azimuthal angles, the dashed and solid curves represent individual and summed GAUSSIAN fits, respectively. The positions of individual transitions determined through the high-resolution PES [23].
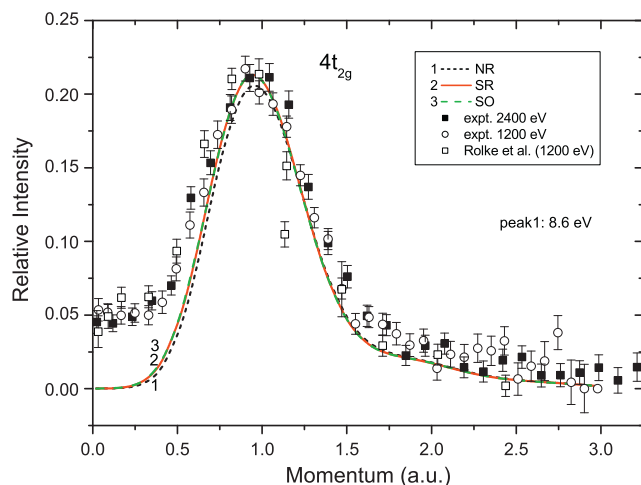
Fig. 2. Experimental and calculated PWIA momentum distributions for the HOMO orbital $4t_{2g}$ of $W(CO)_6$. The theoretical momentum profiles calculated using non-relativistic (NR), scalar relativistic (SR) and spin–orbit relativistic (SO) DFT-B3LYP methods have been convolved with the experimental momentum resolution. The previous experimental data reported by Rolke et al. [5] have been multiplied by a factor of 0.5 for comparing their shape.

Table 1
The population possibilities for each vibrational level at the temperature 310 K.

Vibrational level	Population possibility (%)		
	100.3 (cm^{-1})	120.8 (cm^{-1})	133.5 (cm^{-1})
0	5.2	7.9	9.9
1	9.7	13.6	15.9
2	12.2	15.5	17.1
3	12.8	14.7	15.4
4	12.0	12.6	12.4
5	10.6	10.1	9.3
6	8.8	7.7	6.7
7	7.1	5.6	4.6
8	5.6	4.0	3.1
9	4.3	2.8	2.0

Note: We assumed each vibrational mode is independent. The relative Boltzmann population possibility for the vibrational level n is $(n+1)(n+2)*(exp-nh\nu/KT)$.

Figure 2 shows the experimental momentum distribution for the HOMO $4t_{2g}$ compared with the theoretical results calculated using NR, SR, SO DFT-B3LYP methods under PWIA. The shape of the experimental momentum profile for the HOMO obtained in the present work and the position of the maximum intensity ($p_{max} \approx 1.0$ a.u.) are consistent with the work of Rolke et al. [5]. The HOMO $4t_{2g}$ peak in the high resolution photoelectron spectrum splits into two components with a separation of 0.26 eV, which is due to the spin–orbit interaction as indicated by the SO calculation: a gap of 0.22 eV between $4e_{5/2g}$ and $12u_{3/2g}$ (double group representation). However, the previous EMS work (1.5 eV FWHM) by Rolke et al. [5] and present improved EMS experiment (0.68 eV FWHM) have not achieved the sufficient high energy resolution to resolve these spin–orbit components, thus the summed EMS cross-section was investigated. In Fig. 2, it can be seen that the theoretical momentum distributions of the SR and SO are almost identical, and a little higher than theoretical momentum distribution of NR in the momentum region 0.25 a.u. < p < 1.1 a.u. Compared with theoretical momentum distribution of the NR calculation, both SR and SO relativistic calculations which shift towards the low momentum region provide better descriptions of the observed experimental momentum profile. The HOMO $4t_{2g}$ of $W(CO)_6$ contains a very high contribution from the atomic W 5d ($\sim$60%) orbital, and d orbital expands in position space due to the relativistic effect, so the $4t_{2g}$ HOMO expands in position space. The larger r region usually corresponds to the lower momentum

region, and therefore the intensity of the relativistic calculation in low momentum region is higher than the non-relativistic calculation. The comparison shows that the relativistic effects indeed influence, although not very strongly, the electron momentum distribution of HOMO of $W(CO)_6$.

In general, all calculations can reproduce reasonably well the shape of the momentum profile above $p \sim 0.7$ a.u. including the position of the maximum. However, none of them can explain the significant intensity observed at the lower momentum region. The similar result was also found in the previous EMS work by Rolke et al., where they investigated $Cr(CO)_6$, $Mo(CO)_6$ as well as $W(CO)_6$. They ascribed the high intensity at low momentum to distorted wave effects [6,8,9]. The distorted wave effects can be taken into account in the DWIA calculation instead of the PWIA. Due to the difficulty of the DWIA calculation for a multi-center system (i.e. molecules), the DWIA calculations of the atomic Cr 3d and Mo 4d orbitals was carried out, and the 'turn-up' in the low momentum region was reproduced. Therefore, Rolke et al. deduced that the low momentum 'turn-up' of $W(CO)_6$ was also the result of the distorted wave effects [5]. If this explanation is correct, the turn-up for $W(CO)_6$ should decrease as the impact energy increases [6,8,9]. However, the present experimental results show that the variation of impact energy has little influence on the low momentum 'turn-up'. Therefore, the distorted wave effects alone cannot well explain the unexpected 'turn-up' at low momentum.

One possible reason for the unexpected intensity is the vibrational effects. The bonds between W and CO are relatively weak. The frequency analysis at level of SR-B3LYP/TZ2P predicts that the three lowest vibrational frequencies v are 100.3, 120.8 and 133.5 cm^{-1}. All of these three vibrational frequencies are triply degenerate, which means that each of them have three different vibrational modes, and the only difference is the orientation. Figure 3 shows one vibrational mode for each of the three vibrational fre-
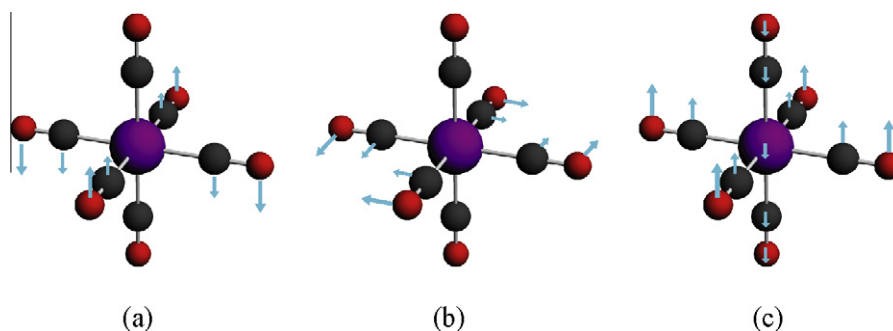

Fig. 3. Different vibrational modes at the frequency (a) 100.3 cm^{-1}, (b) 120.8 cm^{-1} and (c) 133.5 cm^{-1}.
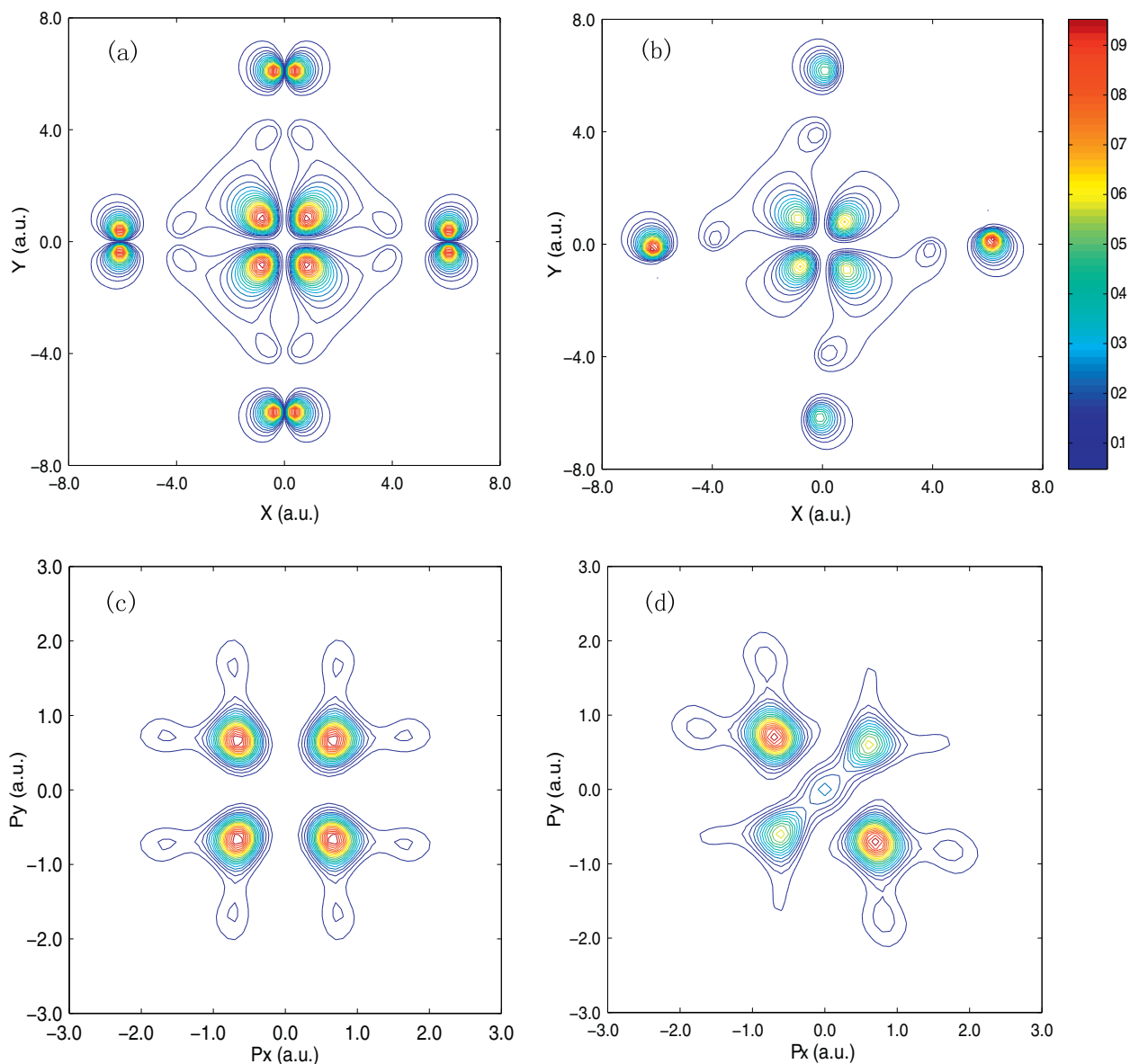
Fig. 4. Orbital electron densities map for HOMO $4t_{2g}$ orbital of equilibrium structure in (a) position space and (c) momentum space, and electron densities map for HOMO orbital (indexed MO_{43}) of one vibrational intermediate structure for $\nu = 120.8$ cm^{-1} in (b) position space and (d) momentum space.

quencies. The real vibrational movements of atoms for each vibrational frequency are linear combination these modes.

These vibrations with low frequencies reflect that the equilibrium structure locates at a rather shallow valley on the potential surface. As a result, the W(CO)$_6$ molecule easily departs from the equilibrium structure at the room temperature (298 K, i.e., 207 cm^{-1}). Table 1 shows the population possibilities for each vibrational level. Here for simplicity, we assume there is no coupling among these modes. It can be seen that the possibility populate at the ground state is less than 10% at our experimental temperature ~310 K. The changes of the geometry structure will result in the changes of the electron momentum distributions of the $4t_{2g}$ orbital. The accurate calculation of the vibrational effects on the momentum distributions needs the full quantum theory [26–29]. It is very complicated considering the size of W(CO)$_6$. For simplification, we illustrated the vibrational effects approximately using the classical method in this Letter. That is, the normalized vibrational displacements of atoms in the W(CO)$_6$ for

each vibrational frequency were used to calculate the momentum distributions.

The nine vibrational intermediate geometries of W(CO)$_6$ (three vibrational frequencies, each frequency contains three kinds of vibrational movements) are constructed from the result of the frequency analysis mentioned above, and then calculated using ADF at the level of SR-B3LYP/TZ2P. The $4t_{2g}$ orbital in equilibrium structure split into three different orbitals in these geometries. For convenience to explain our vibrational correction method, the split orbitals from $4t_{2g}$ for vibrational intermediate structures are numbered as MO_{k3}, MO_{k2}, MO_{k1} ($k = 1, 2, ..., 9$), which are the HOMO, HOMO-1, HOMO-2 for the structure No. k, respectively. The structures Nos. 1–3, 4–6 and 7–9 correspond to $\nu = 100.3, 120.8$ and 133.5 cm^{-1}, respectively.

To explain the vibrational effects on the momentum distributions more intuitively, the two-dimensional orbital wave function in position space and momentum space are plotted using M$_{OMAP}$ program. M$_{OMAP}$ was developed by Prof. Brion's group, University
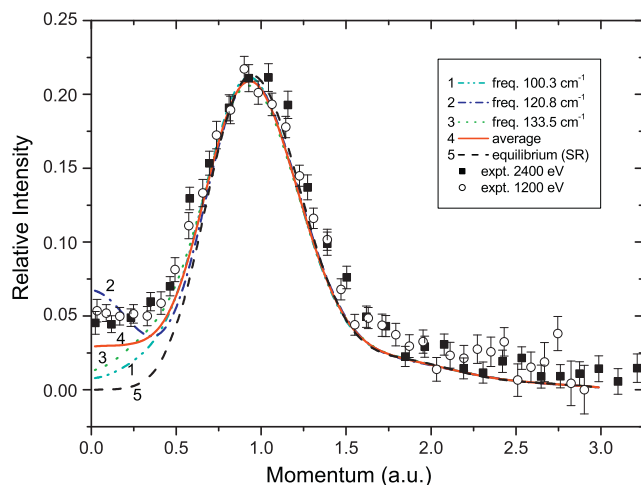
Fig. 5. The momentum distributions of the HOMO orbital $4t_{2g}$ of $W(CO)_6$ with the vibrational correction in comparison with the equilibrium geometry results and experimental results.

of British Columbia. Since the MOMAP program only can handle the GAUSSIAN-type basis sets, not the Slater-type basis sets used in ADF, we recalculate momentum distributions of the equilibrium and the intermediate structures using GAUSSIAN 03W [30] program at the level of B3LYP/LanL2DZ. The relativistic effects have been partly taken into account through the pseudopotential. The calculated results have no evident difference from the ADF calculations. It is found that one vibrational intermediate structure of 120.8 cm^{-1} can remarkably change the momentum distribution at low momentum regions, as shown in Figure 4. Compared with density distribution of the equilibrium structure, vibration breaks the O_h symmetry of $W(CO)_6$. Therefore, the node planes of density distributions disappear in intermediate structures. In contrast with the zero density distribution in momentum origin for the equilibrium structure in Fig. 4c, there is a local maximum intensity around momentum origin for the intermediate structure in Fig. 4d.

Using our NEMS programs incorporating with the ADFCOVT interface, we calculate the theoretical momentum distributions of three orbitals split from $4t_{2g}$ orbital for each geometries, and then summed up together to get the total theoretical momentum distribution for one geometry. The total distributions for the three geometries with the same vibrational frequency are averaged to obtain the correctional distribution of one vibrational frequency. For example, the theoretical momentum profiles of MO_{11}, MO_{12} and MO_{13} are summed up to obtain the theoretical momentum profile for structure No. 1, theoretical momentum profiles for structure Nos. 1–3 are averaged to get the correctional momentum distribution of vibrational frequency 100.3 cm^{-1}. Figure 5 shows the theoretical momentum distribution of $4t_{2g}$ orbital with the vibrational correction in comparison with the SR result in the equilibrium geometry and the experimental data. The solid line is the average of the theoretical momentum distributions for three different vibrational frequencies. It can be seen that the momentum distribution corrected with the vibrational effects reproduces well the significant intensity at lower momentum region. Therefore, we can conclude that the unexpected intensity at the low momentum region for the HOMO is due to the vibrational effects rather than distorted wave effects.

It should be noted that some other effects, such as multi-reference effects [25], Jahn–Teller effects [31] may also change the momentum distributions, as well as the distorted wave effects although not strong. The vibrational effects may interact with these effects together to influence the momentum distribution. It is a challenge for an accurate calculation with all effects.

4. Conclusions

The experimental momentum profiles for the HOMO of $W(CO)_6$ have been obtained at impact energies of 1200 and 2400 eV. The theoretical non-relativistic, scalar relativistic and spin–orbit relativistic DFT-B3LYP method are compared with experimental momentum distributions. The relativistic calculations provide a little better descriptions for experiments than the non-relativistic calculation, which indicate relativistic effects influence the electron density in HOMO $4t_{2g}$ of $W(CO)_6$, even not strongly. The semi-quantitative calculation indicated that the low frequency vibration of $W(CO)_6$ can evidently change the momentum profile. We suggested that the unexpected intensity in the low momentum region for the HOMO $4t_{2g}$ is likely due to the vibrational effects.

Acknowledgements

References

[1] I.E. McCarthy, E. Weigold, Rep. Prog. Phys. 54 (1991) 789.
[2] M.A. Coplan, J.H. Moore, J.P. Doering, Rev. Mod. Phys. 66 (1994) 985.
[3] E. Weigold, I.E. McCarthy, Electron Momentum Spectroscopy, Kluwer Academic Plenum Publishers, New York, 1999.
[4] F.A. Cotton, G. Wilkinson, Advanced Inorganic Chemistry, Wiley-Interscience, New York, 1988.
[5] J. Rolke, Y. Zheng, C.E. Brion, S.J. Chakravorty, E.R. Davidson, I.E. McCarthy, Chem. Phys. 215 (1997) 191.
[6] C.E. Brion, Y. Zheng, J. Rolke, J.J. Neville, I.E. McCarthy, J. Wang, J. Phys. B: At. Mol. Phys. 31 (1998) L223.
[7] M. Takahashi, T. Saito, J. Hiraka, Y. Udagawa, J. Phys. B: At. Mol. Phys. 36 (2003) 2539.
[8] X.G. Ren, C.G. Ning, J.K. Deng, S.F. Zhang, G.L. Su, F. Huang, G.Q. Li, Phys. Rev. Lett. 94 (2005) 163201.
[9] C.G. Ning, X.G. Ren, J.K. Deng, G.L. Su, S.F. Zhang, G.Q. Li, Phys. Rev. A 73 (2006) 022704.
[10] K.L. Nixon, W.D. Lawrance, M.J. Brunger, Chem. Phys. Lett. 474 (2009) 23.
[11] J.F. Gao, D.H. Madison, J.L. Peacher, Phys. Rev. A 72 (2005) 032721.
[12] C.J. Colyer, M.A. Stevenson, O. Al-Hagan, D.H. Madison, C.G. Ning, B. Lohmann, J. Phys. B: At. Mol. Phys. 42 (2009) 235207.
[13] L.R. Hargreaves, C. Colyer, M.A. Stevenson, B. Lohmann, O. Al-Hagan, D.H. Madison, C.G. Ning, Phys. Rev. A 80 (2009) 062704.
[14] K. Liu, C.G. Ning, J.K. Deng, Phys. Rev. A 80 (2009) 022716.
[15] X.G. Ren, C.G. Ning, J.K. Deng, S.F. Zhang, G.L. Su, F. Huang, G.Q. Li, Rev. Sci. Instrum. 76 (2005) 063103.
[16] C.G. Ning, S.F. Zhang, J.K. Deng, K. Liu, Y.R. Huang, Z.H. Luo, Chin. Phys. B 17 (2008) 1729.
[17] P. Duffy, D.P. Chong, M.E. Casida, D.R. Salahub, Phys. Rev. A 50 (1994) 4707.
[18] Amsterdam Density Functional (ADF) Code, Release 2008, Vrije Universiteit, Amsterdam, The Netherlands.
[19] C. Lee, W. Yang, R.G. Parr, Phys. Rev. B 37 (1988) 785.
[20] E. Vanlenthe, E. Baerends, J. Snijders, J. Chem. Phys. 101 (1994) 9783.
[21] A.W. Ehlers, G. Frenking, J. Chem. Soc. Chem. Commun. (1993) 1709.
[22] C.G. Ning et al., Chem. Phys. 343 (2008) 19.
[23] B.R. Higginson, D.R. Lloyd, P. Burroughs, D.M. Gibson, A.F. Orchard, J. Chem. Soc. Faraday Trans. II 69 (1973) 1659.
[24] P. Duffy, M.E. Casida, C.E. Brion, D.P. Chong, Chem. Phys. 159 (1992) 347.
[25] K. Hirao (Ed.), Recent Advances in Multireference Methods, World Scientific, Singapore, 1999.
[26] B.P. Hollebone, J.J. Neville, Y. Zheng, C.E. Brion, Y. Wang, E.R. Davidson, Chem. Phys. 196 (1995) 13.
[27] F. Morini, B. Hajgato, M.S. Deleuze, C.G. Ning, J.K. Deng, J. Phys. Chem. A 112 (2008) 9083.
[28] C.G. Ning et al., J. Phys. B: At. Mol. Phys. 41 (2008) 175103.
[29] B. Hajgato, M.S. Deleuze, F. Morini, J. Phys. Chem. A 113 (2009) 7138.
[30] M.J. Frisch, GAUSSIAN 03, Revision E.01.
[31] Z.J. Li, X.J. Chen, X. Shan, T. Liu, K.Z. Xu, J. Chem. Phys. 130 (2009) 054302.